https://doi.org/10.31436/iiumej.v27i2.4134

A Comprehensive Framework of Ant Colony Optimization for Optimal Control of Upper Extremity Rehabilitation Robot

M. KAMRAN JOYO[1,*], IZANOORDINA AHMAD[1], KUSHSAIRY ABDUL KADIR[1], TALHA AHMED KHAN[2], NOAMAN M. NOAMAN[3]

[1]*Electronics Engineering Department, Universiti Kuala Lumpur British Malaysian Institute, 53100, Malaysia*
[2]*Cyber Security and Technological Convergence, Malaysian Institute of Information Technology (MIIT), Universiti Kuala Lumpur, Kuala Lumpur, Malaysia*
[3]*College of Engineering, University of Technology, Bahrain, Kingdom of Bahrain*

**Corresponding author: M. Kamran Joyo (muhammadkamran@unikl.edu.my)*

(Received: 14 January 2026; Accepted: 21 April 2026; Published online: 10 May 2026)

ABSTRACT: Passive rehabilitation of the upper limb requires precise joint positioning to facilitate motor recovery and ensure patient safety. For a two-degree-of-freedom (DOF) elbow robot, the primary challenge is unwanted disturbances arising from human coupling and voluntary and involuntary forces applied by the subject. This study addresses this issue by proposing a comprehensive control framework based on a nature-inspired meta-heuristic approach. The robot dynamics were obtained using the Lagrangian formulation, which was then combined with a realistic actuator model, yielding a closed-loop transfer function that describes system behavior. A two-degree-of-freedom (2-DOF) PID controller was used as the position controller. To determine the optimal PID parameters, an ant colony optimization (ACO) algorithm is used with an appropriate performance index to select the PID parameter values. The resulting ACO-based PID controller showed significant improvement over the conventional Ziegler–Nichols (Z-N) approach, as it could reject significant patient-induced forces, maintain the joint trajectory with the reference, and remain stable even under perturbations. Simulations were performed, confirming that the optimized controller delivers smooth, precise movements, reduces tracking error, and enhances the safety of passive rehabilitation procedures.

ABSTRAK: Pemulihan secara pasif di bahagian anggota atas pesakit memerlukan kedudukan sendi yang tepat bagi memudahkan pemulihan motor pesakit daripada bahaya atau cedera. Manakala pada robot siku dua darjah kebebasan (DOF), cabaran utama ialah mengelakkan gangguan yang tidak diingini oleh manusia dan daya sukarela atau tidak sukarela yang dikenakan oleh subjek. Kajian ini mencadangkan rangka kerja kawalan komprehensif berdasarkan pendekatan meta-heuristik yang diilham oleh alam semula jadi. Dinamik robot diwujudkan dengan menggunakan rumusan Lagrangian, diikuti dengan gabungan model penggerak realistik, agar dapat menghasilkan fungsi pemindahan gelung tertutup yang boleh menggambarkan tingkah laku sistem. Pengawal PID 2-DOF pula digunakan sebagai pengawal kedudukan. Bagi mencapai parameter optimum PID, algoritma Pengoptimuman Koloni-Semut (ACO) digunakan dengan indeks prestasi yang sesuai agar dapat memilih PID paling optimum. Pengawal PID berasaskan ACO yang terhasil mengatasi pendekatan Ziegler Nichols (Z-N) konvensional, kerana ia mempunyai keupayaan menolak daya teraruh pesakit yang ketara sambil mengekalkan trajektori bersama rujukan dan kekal stabil walaupun ketika gangguan. Simulasi yang dijalankan dalam kajian ini mengesahkan bahawa pengawal yang

https://doi.org/10.31436/iiumej.v27i2.4134

dioptimumkan berjaya mencapai pergerakan yang lebih lancar, tepat, seterusnya mengurangkan ralat pengesanan serta mempromosi keselamatan prosedur pemulihan pasif.

KEYWORDS: *Ant Colony Optimization, Rehabilitation Robot, PID, Ziegler Nichols*

1. INTRODUCTION

Stroke is the most common cause of long-term disability, and about half of the patients are left with upper limb motor impairment, which significantly impairs their quality of life [1, 2]. The process of recovery depends on intensive, repetitive, and task-specific exercises, which must begin in the early stages of the illness, during the acute and subacute stages [3]. Among rehabilitation modalities, passive range-of-motion exercises constitute a foundational therapeutic approach, particularly for patients with severe motor deficiencies who are unable to voluntarily initiate limb movements. These exercises prevent musculoskeletal problems, reduce spasticity, and facilitate the restoration of the functionality of disabled limbs [4]. Post-stroke therapy has been transformed by robotic rehabilitation systems, which provide specific and extensive repetitive movements with a significant reduction in the workload of therapists, allowing prolonged training sessions, and evidence demonstrates that extensive interventions significantly improve motor recovery [5].

Robot-assisted therapy offers advantages similar to those of conventional physiotherapy, providing consistent repeatability and performance tracking [6, 7]. Furthermore, combining passive range-of-motion exercises with visual and cognitive feedback mechanisms enhances motivation and engagement in therapy. Studies using functional near-infrared spectroscopy support the idea that robot-assisted therapy promotes neuroplasticity, thereby activating motor cortical regions and enhancing neural connections involved in functional recovery. The efficacy of robotic rehabilitation largely depends on the characteristics of the motion control employed within the system. In passive rehabilitation systems, the robot must track predefined trajectories with high precision, at the same time compensating for the mechanical properties and reactive forces exerted by the patient's limb [8].

Modern rehabilitation robots are employed in diverse configurations, including end-effector and exoskeleton-based structures, each presenting distinctive control challenges [9, 10]. These systems must accurately track predefined paths and, at the same time, handle variable human loads caused by heterogeneity in limb mass, involuntary contractions, and varying muscular flexibility [11]. The interaction between humans and robots is dynamic, leading to significant uncertainty in controller design. Such exercises prevent musculoskeletal problems, reduce spasticity, and facilitate the restoration of function in disabled limbs, thereby underscoring the need for robust control strategies [12]. The safety factors in physical HRI are the most important because excessive forces applied to soft and musculoskeletal tissues can cause injury, especially when applied for prolonged durations. However, small forces can be dangerous because of continuous contact and cyclic motion [9]. These human-coupled disturbances undermine the accuracy of position tracking, potentially leading to suboptimal therapeutic outcomes or patient discomfort.

Classical control methods for rehabilitation robots typically employ proportional-integral-derivative (PID) controllers tuned using heuristic methods such as Ziegler-Nichols. Despite the simplicity of PID control and its broad scope, heuristic-based parameterization is often unable to support multi-objective rehabilitation requirements, such as achieving rapid convergence, reducing overshoot, and maximizing disturbance rejection [13, 14].

https://doi.org/10.31436/iiumej.v27i2.4134

Existing studies have explored metaheuristic optimization techniques, which are recognized as effective methods for solving complex controller tuning problems. These include ant colony optimization (ACO), which has proven especially effective for finding optimal PID parameters by simulating ant colony foraging dynamics. The ACO exhaustively searches the parameter space by means of probabilistic exploration and exploitation to effectively identify near-optimal solutions [15]. Despite this potential, existing ACO-based rehabilitation control studies often suffer from limited comparative evaluations across different performance indices [16]. Furthermore, unlike previous studies that predominantly adapt discrete pheromone models to continuous tuning, this study employs ACO using a Gaussian kernel probability density function. This facilitates the exploration of search parameters in continuous space.

The contributions of this study include a dynamic and linearised model of a 2-DOF rehabilitation exoskeleton integrated with an actuator model. Second, a 2-DOF-PID architecture was applied to decouple reference tracking and disturbance in the presence of human-induced torques. Third, an ACO framework for a continuous domain was employed to tune the controller parameters using multiple integral performance indices. Fourth, a disturbance model was introduced, and robustness was assessed against sustained involuntary human-applied torques.

The remainder of this paper is organized as follows: Section 2 presents the dynamic modeling and controller design methodology. Section 3 presents the simulation results and optimization analysis; Section 4 provides a comprehensive comparative evaluation and discussion of the findings; and Section 5 concludes the paper with recommendations for future research directions.

2. MATERIALS AND METHODS

2.1. Overview of the RAX-1 Exoskeleton System

RAX-1 is an exoskeleton device developed for upper limb rehabilitation. The system is engineered to operate in coordination with the human forelimb, mimicking natural movement sequences to rehabilitate neuromuscular function. The human forelimb comprises nine degrees of freedom (DOFs), excluding the finger joints. In this study, the focus is on the elbow (humeroulnar) joint, which mainly involves flexion and extension movements and provides rotation of the forearm in its interaction with the humeroradial and proximal radioulnar joints.

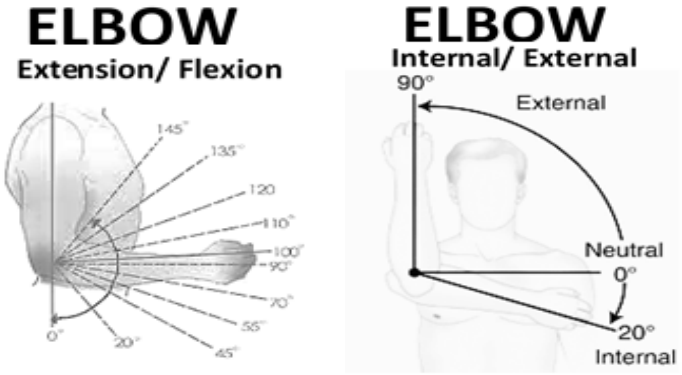

Figure 1. Elbow Extension/ Flexion and Elbow Internal/ External Rotation

Figure 1 depicts the principal motions of the elbow joint complex, and Table 1 lists the corresponding ranges of motion in healthy subjects [17]. These motion parameters were implemented as reference trajectories within the RAX-1 exoskeleton. The overall RAX-1

https://doi.org/10.31436/iiumej.v27i2.4134

configuration supports five DOFs, enabling exercises for the shoulder, elbow, and wrist. However, the shoulder and wrist joints were not actuated and were excluded from the control model, whereas only the elbow joints were actively controlled. A 3D model of the robot manipulator is illustrated in Figure 2.

Table 1. Range of Motion

Limb	Therapeutic exercise	ROM of Limb
Elbow	Extension/ Flexion	0° - 145°
	Internal/ External Rotation	-20° - 90°

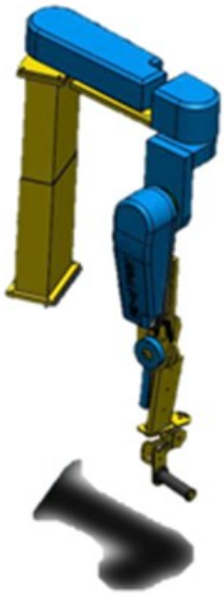

Figure 2. 3D CAD Model of RAX-1

2.2. Modeling using the Euler–Lagrange Approach

The dynamic model of the robotic manipulator was derived using the Euler–Lagrange formulation, which relates the joint positions and velocities to the system's kinetic and potential energies. This approach generalizes Newtonian mechanics to systems with position-dependent constraints. The Lagrangian L is defined as:

$$L = K - P \tag{1}$$

K and P denote the kinetic and potential energies, respectively. The generic mathematical expression that represents the motion of the jth joint is written as

$$\frac{d}{dt}\left(\frac{\partial L}{\partial \dot{q}_j}\right) - \frac{\partial L}{\partial q_j} = \tau_j \tag{2}$$

where q_j represents the generalized coordinate, and τ_j is the required joint torque. The nonlinear dynamics derived above are linearized around the equilibrium point defined by the model initial conditions, i.e., $(q = 0, \dot{q} = 0)$ yielding a linear state-space representation $\dot{x} = Ax + Bu(t) + B_{hd}\tau_{hd}(t), y = Cx + Du(t)$, where $x = [q\ \dot{q}]^T$ suitable for control design. Since both actuator and human torque act on the same physical joint, the disturbance distribution matrix is $B_{hd} = B$. The human disturbance is defined as two input external torque vector $\tau_{hd}(t) = [\tau_{hd_1} \quad \tau_{hd_2}]^T$ representing the involuntary or resistive human interaction acting about the flexion/extension and forearm pronation/supination axes. The human

https://doi.org/10.31436/iiumej.v27i2.4134

disturbance torque was modeled as constant external load applied at each joint, with magnitudes selected as a fixed percentage of the actuator rated torque. These terms are defined as

$$\tau_{hd_1}(t) = \begin{cases} 0 & for\ t < t_d \\ \tau_{d_1} & for\ t > t_d \end{cases} \quad (3)$$

$$\tau_{hd_2}(t) = \begin{cases} 0 & for\ t < t_d \\ \tau_{d_2} & for\ t > t_d \end{cases} \quad (4)$$

where τ_{d_1} and τ_{d_2} represents the abrupt, sustained nature of involuntary muscle activation, spastic, and resistive behavior during passive rehabilitation rather than short-duration impulsive disturbances. The linearized model expresses the dynamics of a system as the relationship among velocity, position, and torque, which forms the basis for controller implementation.

$$A = \begin{bmatrix} 0 & 1 & 0 & 0 \\ -30.351 & 0 & 0.0397 & 0 \\ 0 & 0 & 0 & 1 \\ 0.1685 & 0 & -30.023 & 0 \end{bmatrix}, \quad B = \begin{bmatrix} 0 & 0 \\ 6.8916 & 0.0028 \\ 0 & 0 \\ 0.0028 & 6.7582 \end{bmatrix},$$

$$C = \begin{bmatrix} 1 & 0 & 0 & 0 \\ 0 & 0 & 1 & 0 \end{bmatrix}, \quad D = [0 \quad 0 \quad 0 \quad 0] \quad (5)$$

The exoskeleton joint is actuated by a DC motor that converts electrical input into rotational mechanical torque. Mechanical rehabilitation prefers DC motors owing to their low inertia, high torque density, and ability to control speed. The internal motor model is defined as follows:

$$V_a = L_a \frac{di_a}{dt} + R_a i_a + K_b \omega \quad (6)$$

$$T_m = K_\tau i_a = J \frac{d\omega}{dt} + B_m \omega + T_L \quad (7)$$

J is the inertia of the rotor in the above formula; B_m is the viscous damping coefficient; K_τ is the torque constant; K_b is the back EMF constant, and L_a, R_a are the armature inductance and resistance, respectively. In the case of $L_a \ll R_a$, the inductance term is very small and can be omitted, and the model is reduced to a first-order approximation. The motor is connected to a harmonic gear reduction unit to boost the torque output. Table 2 [18] provides detailed parameters.

Table 2. Motor Parameters

Parameters	Values
L_a (Henry)	2.6400e-04
R_a (ohms)	0.363
K_m (Torque Constant)	0.0705
J (Kg.m2/s2)	3.1212e-05
K_f (Nms)	8.66301e-03
K_b (back emf constant)	8.66301e-03
n (Gear Ratio)	75

It is important to acknowledge the limitations of the developed model. First, the robot dynamics were linearised around the equilibrium point defined by the model's initial conditions. Second, the human disturbance torque was modeled as a constant, sustained load

applied at each joint. Although this effectively simulates spasticity or a patient's persistent resistive force, it does not capture the full complexity of time-varying or impulsive interactions.

2.3. Control Algorithm

2.3.1. Two-Degree-of-Freedom PID Controller

A 2-DOF proportional–integral–derivative (PID) controller is incorporated to provide accurate tracking of the reference and to reject all disturbances. The controller continuously computes the difference between the desired and actual positions and adjusts the control signal accordingly [26]. The controller is mathematically expressed as

$$u(t) = K_p(b.r - y) + K_i(r - y)s^{-1} + K_d \frac{N}{1+Ns^{-1}}(c.r - y) \quad (8)$$

where K_p, K_i, K_d are proportional, integral, and derivative gains. In order to improve the flexibility and transient performance, the setpoint weighting parameters b and c are incorporated for the independent tuning of the proportional and derivative actions. MATLAB's 2-DOF PID block is utilized for implementation, allowing the adjustment of K_p, K_i, K_d, b, c, and filter coefficient N. This arrangement enables independent tuning of transient and steady-state responses for passive rehabilitation control.

2.3.2. Ant Colony Optimization for Continuous Domains

Ant colony optimization (ACO) is a population-based metaheuristic inspired by the foraging behavior of ant colonies, in which solutions are generated through the guided exploration of pheromone trails. To ensure continuous optimization, the pheromone model used by ACO employs a Gaussian kernel probability density function (PDF), which allows ants to sample continuous decision spaces instead of discrete solution elements [19]. The Gaussian kernel PDF is a weighted sum of the Gaussian function, which is defined as

$$G^i(x) = \sum_{l=1}^{k} \Omega_l g_l^i(x) = \sum_{l=1}^{k} \Omega_l \frac{1}{\sigma_l^i \sqrt{2\pi}} e^{-\left(\frac{(x-\mu_l^i)^2}{2\sigma_l^{i\,2}}\right)} \quad (9)$$

In the above formula, Ω is the weight vector of individual Gaussian functions, μ is the mean vector, and σ is the standard deviation. Solutions that are in an archive of size k parameterize this kernel, which stores the best solutions found during the search process. The ongoing ACO comprises three key elements:

Construction of Solution: Each ant constructs a solution through n construction steps for n decision variables. At Step i, the ant samples a variable via a two-stage process: first selecting a Gaussian function from the kernel with probability proportional to its weight.

$$P_l = \frac{\omega_l}{\sum_{r=1}^{k} \omega_r} \quad (10)$$

Then, samples were drawn from the selected Gaussian distribution. The standard deviation at the construction step i is computed as:

$$\sigma_l^i = \xi \sum_{e=1}^{k} \frac{\left|s_e^i - s_l^i\right|}{k-1} \quad (11)$$

where ξ is the pheromone evaporation parameter that controls convergence speed: larger values promote exploration while smaller values favor exploitation.

Pheromone Update: The solution archive maintains k high-quality solutions that define the PDF. After each iteration, newly generated solutions are added to the archive, and an equal number of the worst-performing solutions are removed, preserving the archive size and ensuring that the PDF reflects promising regions of the search space.

Daemon Actions: This optional component updates the best-found solution and implements termination criteria, typically based on the maximum iterations or convergence thresholds. The ACO parameters and values used in this study are presented in Table 3.

Table 3. ACO Parameters

Parameters	Values
Archive Size	20
Number of iterations	50
Sample Size	10
$\boldsymbol{q}$ (Selection pressure)	0.5
$\boldsymbol{\zeta}$ (Deviation distance ratio)	1

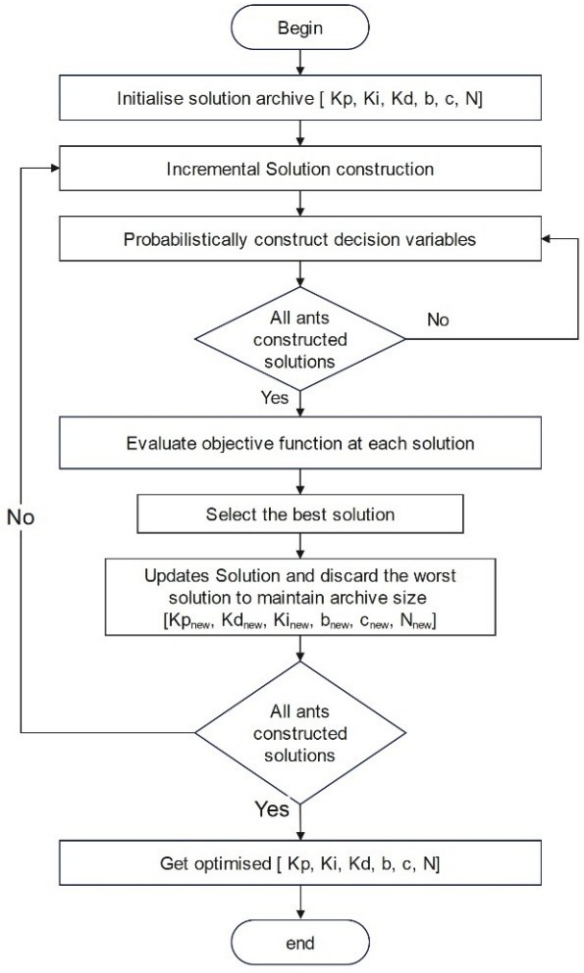

Figure 3. ACO metaheuristic framework for continuous optimization

The system was simplified to a linearized subsystem representing the elbow joint. A dedicated control loop equipped with saturation limits was used to regulate the robot's motion. A step input was applied to the elbow-joint model to assess the system response and evaluate the controller's overall performance. Figure 4 shows a schematic of the proposed control approach for utilizing the ACO algorithm for the elbow joint.

https://doi.org/10.31436/iiumej.v27i2.4134

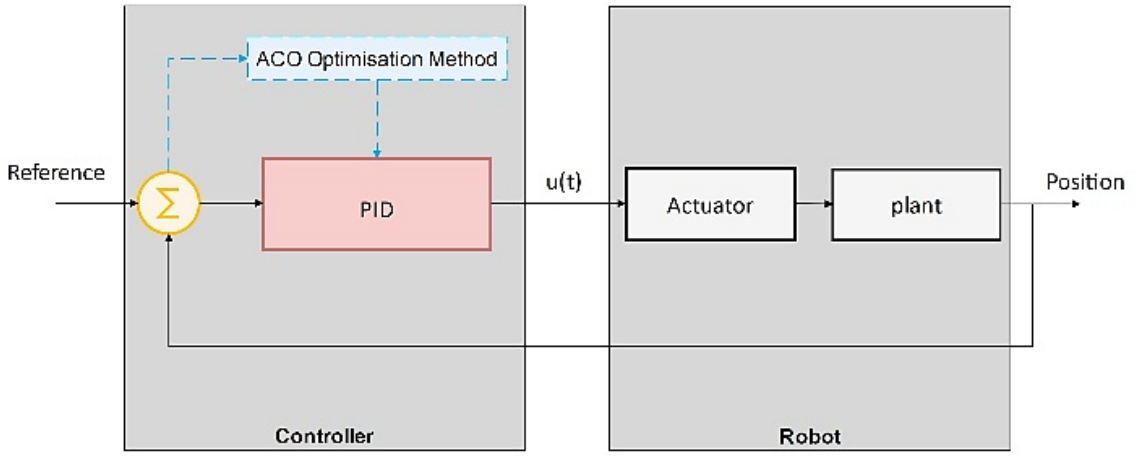

Figure 3. ACO-based proposed control structure

The effectiveness of model-based control systems depends on the selection of an appropriate performance index that encapsulates both the design criteria and system limitations. The performance index (objective or cost function) provides a measurable benchmark for optimization algorithms to minimize or maximize. A well-chosen performance index affects not only the algorithm's convergence behavior but also significantly influences the quality of the resulting controller parameters and, ultimately, the system's practical performance.

This study offers a comparative analysis of four integral-based performance indices to determine the most appropriate performance index for the upper-limb rehabilitation robotic system under study. The performance indices are Integral Squared Error (ISE), Integral Time Squared Error (ITSE), Integral Absolute Error (IAE), and Integral Time Absolute Error (ITAE). These performance indices are selected for their effectiveness in control systems for reference tracking and disturbance rejection. These performance measures have varying influences on the control elements. For example, the ISE and IAE aim to reduce the cumulative tracking error, whereas the time-weighted indices of ISE and ITAE apply a more severe punishment for extended deviations from the intended path. This difference plays a pivotal role in rehabilitation settings, where errors in reference tracking may impair patients' muscles. The objective here is to identify the performance index that can most effectively address the major goals, including correcting motion tracking, restricting overshoot, and improving disturbance rejection, to control unforeseen dynamics and forces exerted by the patient. The mathematical formulas for these functions are explained below.

$$ISE = \int e^2 dt \tag{12}$$

$$IAE = \int |e| dt \tag{13}$$

$$ITSE = \int t.e^2 dt \tag{14}$$

$$ITAE = \int t.|e| dt \tag{15}$$

The controller tuning process accounts for robustness to ensure stable closed-loop behavior in the presence of uncertainties, such as external disturbances. This is achieved using the maximum sensitivity function as a measure of robustness. It is defined as

$$M_s = \max_{\omega} |S(j\omega)| = \max_{\omega} \frac{1}{|1 - C_y(j\omega)P(j\omega)|} \tag{16}$$

where $S(j\omega)$ denotes the sensitivity function and $|S(j\omega)| \leq M_s$. The sensitivity function indicates how feedback affects the system output in response to disturbances. Disturbances are amplified when $|S(j\omega)| > 1$ and are attenuated when $|S(j\omega)| < 1$. Therefore, lower Ms values indicate greater robustness, as the system becomes less sensitive to uncertainties and external perturbations. The values of M_s ranging from 1.2 to 2.0 provides reasonable robustness [20].

3. RESULTS

An extensive set of simulation experiments was conducted in MATLAB to evaluate the effectiveness of the proposed control algorithm. A comparative study was conducted based on parameter analysis of the PID controller optimized using ACO and the conventional Z-N method. Ziegler-Nichols was selected as the baseline for comparison, largely because it is one of the most widely recognized classical approaches in the literature and offers an established standard. Several studies in rehabilitation systems have employed Z-N as their reference standard, enabling comparison. More importantly, Z-N is heuristic and does not optimize for specific integral-error criteria or disturbance rejection; it serves as an appropriate performance baseline against which the advantages of the ACO-based optimization method can be demonstrated. Table 4 lists the PID parameter ranges, and Table 5 presents the PID parameters obtained using ACO and Z-N. The analysis was narrowed to the motions of the elbow: extension and flexion, with internal and external rotation of the forearm.

Table 4. Parametric Constraints used for ACO and Z-N

Controller	Parameters	Elbow (E/F)	Elbow (I/E)
Ant colony	K_p	$0.01 < K_p < 10$	$0.01 < K_p < 10$
	K_i	$0.01 < K_i < 10$	$0.01 < K_i < 10$
	K_d	$0.01 < K_d < 10$	$0.01 < K_d < 10$
	b	$0.01 < b < 1$	$0.01 < b < 1$
	c	$0.01 < c < 1$	$0.01 < c < 1$
	N	$1 < N < 200$	$1 < N < 200$
Ziegler Nichols	K_u	4.5	5.4
	T_u	2.1	2.1

Table 5. Optimised parameters

Controller	Performance Index	Kp	Ki	Kd	b	c	N
		Elbow Extension/ Flexion					
PID-ACO	ISE	**2**	**1.9305**	**1.2024**	**0.47021**	**1.469**	**77.2565**
	IAE	**1.9799**	**2**	**0.59161**	**0.44925**	**0.93431**	**78.0639**
	ITSE	**1.9971**	**1.5836**	**1.1014**	**0.4737**	**1.5400**	**89.6019**
	ITAE	**1.9535**	**1.6479**	**0.4565**	**0.4388**	**0.8867**	**80.1878**
Ziegler-Nichols	-	2.16	3.6	0.324	1	1	100
		Elbow Internal/ External Rotation					
PID-ACO	ISE	1.1615	0.0001	2	0.9988	1.5588	48.1113
	IAE	2	1.4005	1.3777	0.8391	1.7570	111.3369
	ITSE	1.9328	1.7273	2	0.9141	1.7241	52.3570
	ITAE	1.8621	1.2025	1.2285	0.8678	0.9470	75.7466
Ziegler-Nichols	-	3.24	3.0857	0.8505	1	1	100

Figures 5 to 10 illustrate the step responses of the elbow joint using the IAE, ITAE, ISE, and ITSE performance indices, along with the conventional Ziegler–Nichols controller, for both joints. Figure 5a and 5b illustrate a step response of the elbow joint using IAE for flexion/extension and internal/external rotation, respectively. Figure 6a and 6b illustrate a step

https://doi.org/10.31436/iiumej.v27i2.4134

response of the elbow joint using ISE for flexion/ extension and internal/ external rotation, respectively.

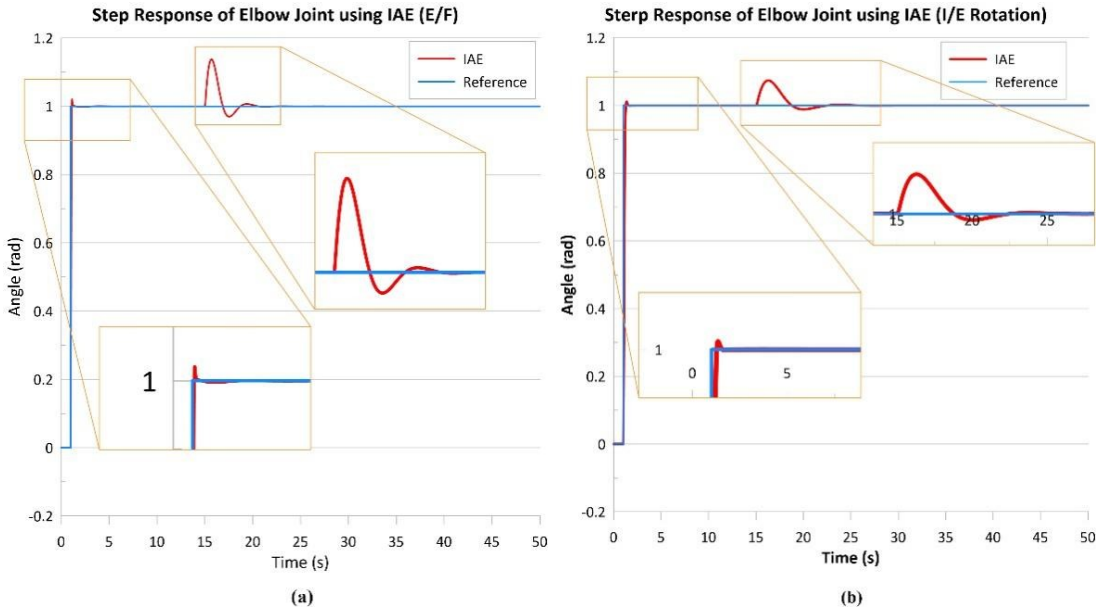

Figure 1. Step response of RAX-1 Elbow Joint using IAE optimized PID control (a) Extension/ Flexion, (b) Internal/ External Rotation

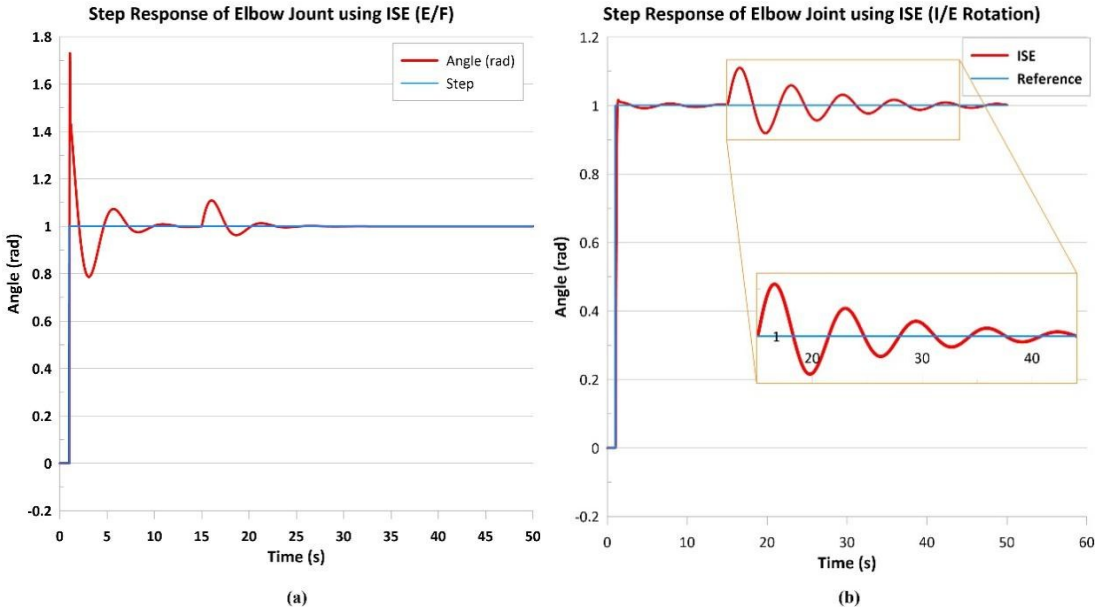

Figure 2. Step response of RAX-1 Elbow Joint using ISE optimized PID control (a) Extension/ Flexion, (b) Internal/ External Rotation

Figures 7a and 7b illustrate the step response of the elbow joint using ITAE for flexion/extension and internal/external rotation, respectively. Figure 8a and 8b illustrate a step response of the elbow joint using ITSE for flexion/ extension and internal/ external rotation, respectively.

https://doi.org/10.31436/iiumej.v27i2.4134

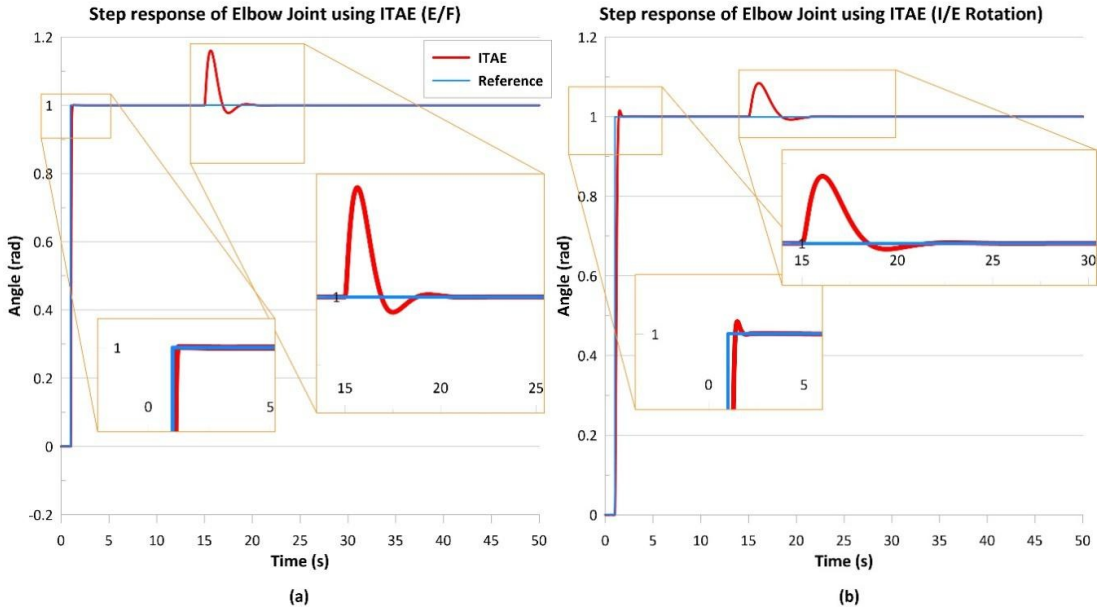

Figure 3. Step response of RAX-1 Elbow Joint using ITAE optimized PID control (a) Extension/ Flexion, (b) Internal/ External Rotation

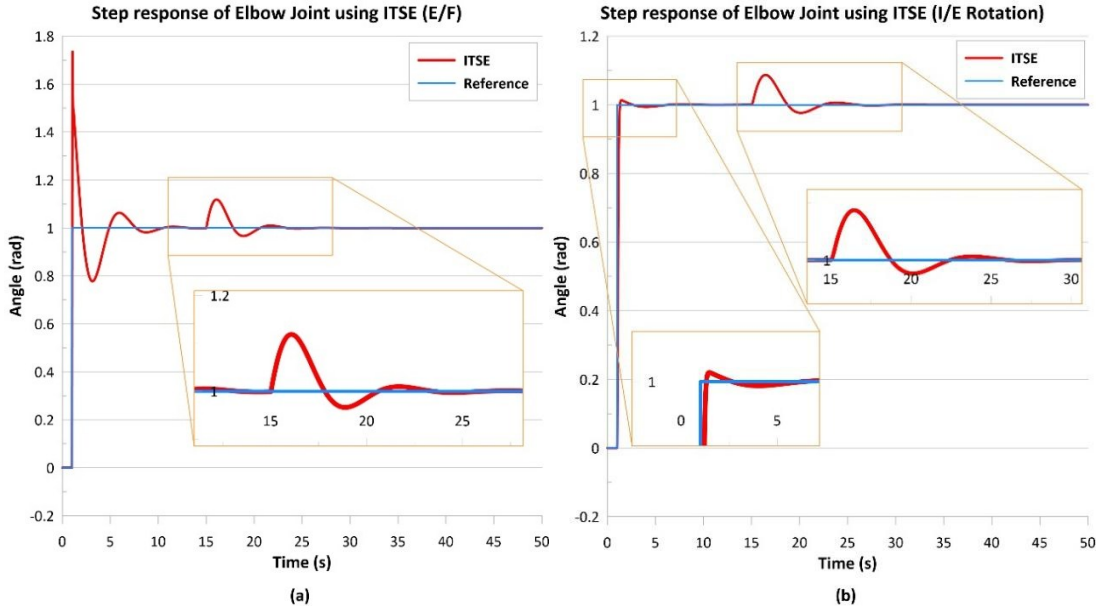

Figure 4. Step response of RAX-1 Elbow Joint using ITSE optimized PID control (a) Extension/ Flexion, (b) Internal/ External Rotation

Figures 9a and 9b illustrate the step response of the elbow joint using Z-N for flexion/extension and internal/external rotation, respectively.

https://doi.org/10.31436/iiumej.v27i2.4134

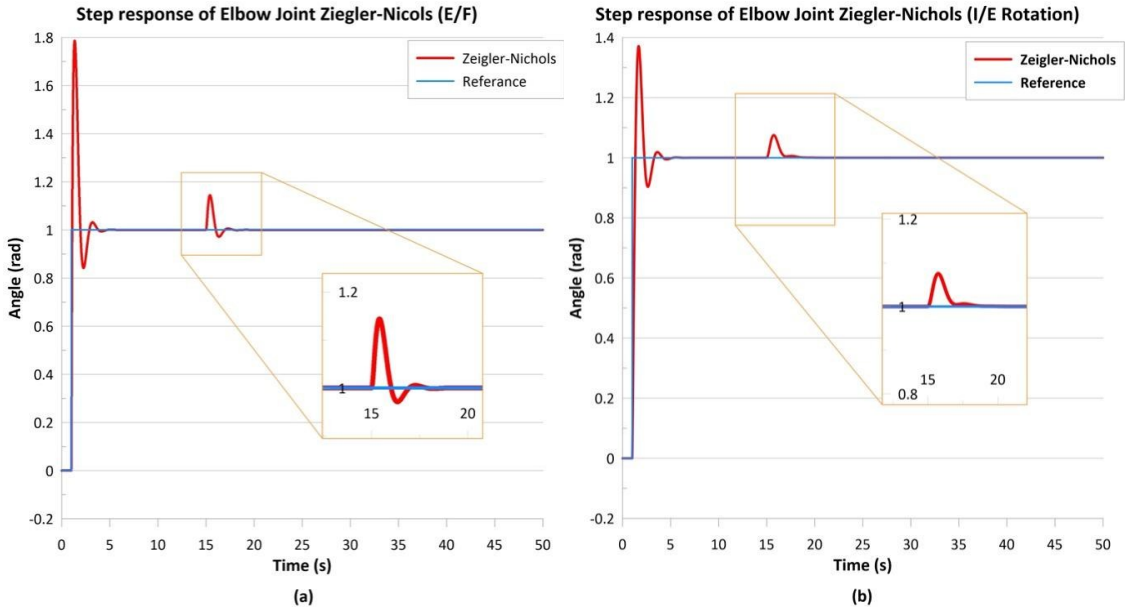

Figure 5. Step response of RAX-1 Elbow Joint Ziegler-Nichols (a) Extension/ Flexion, (b) Internal/ External Rotation

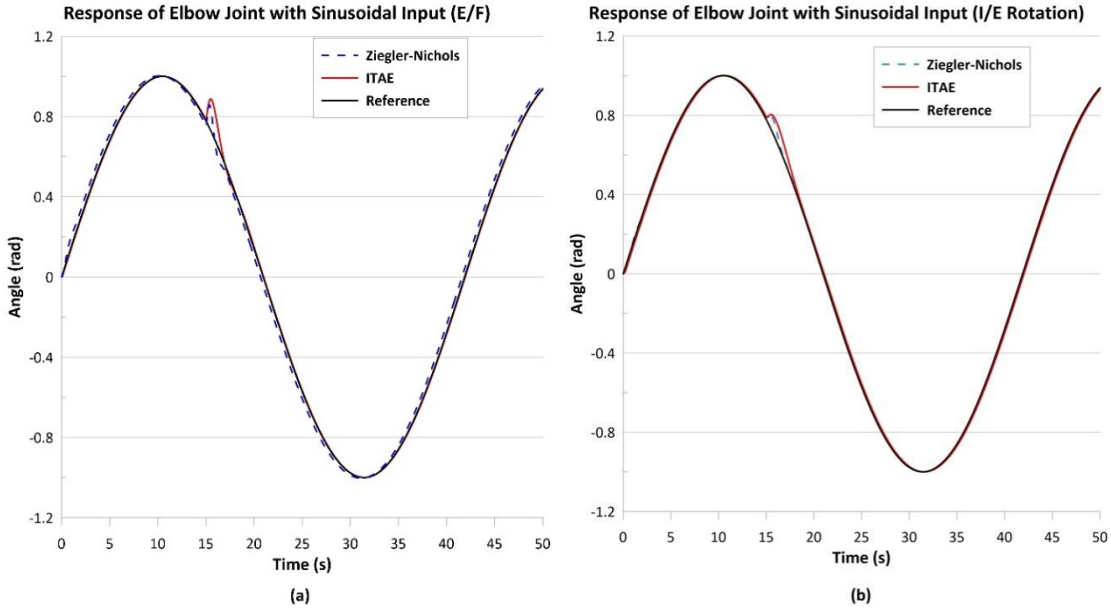

Figure 6. Sinusoidal tracking of RAX-1 Elbow Joint using ITAE optimized PID control and Ziegler-Nichols

Figures 10a and 10b show a comparison of the tracking performance of the ITAE-based ACO and Z-N tuned controllers for elbow joint flexion/extension and internal/external rotation when subjected to a sinusoidal reference trajectory.

4. DISCUSSION

Figure 5a and 5b illustrate the step response of the elbow joint under IAE-based ACO-PID control for flexion/extension and internal/external rotation, respectively. The ACO-tuned controller with IAE exhibits an immediate rise, minimal overshoot, and a stable settling region, demonstrating smooth tracking of the reference signal. The small, highlighted insets show the

minimal steady-state error and consistent transient performance throughout the simulation period, with effective rejection of the step disturbance introduced at 15s. This disturbance was intentionally introduced to represent voluntary or involuntary forces that a subject may apply during rehabilitation exercises. The controller maintains stable tracking despite this perturbation, demonstrating its ability to compensate for human-generated disturbances while preserving smooth and safe elbow joint motion. Figure 6a and 6b illustrate the step response of the elbow joint using ITAE for flexion/extension and internal/external rotation, respectively. The ACO-tuned controller with ITAE presents a similar stable response with slightly faster convergence than that with IAE. The ITAE criterion minimizes sustained oscillations by penalizing prolonged errors over time, resulting in a smoother trajectory closer to the reference. Figures 7a and 7b illustrate a step response of the elbow joint using ISE for flexion/extension and internal/external rotation, respectively. Figures 8a and 8b illustrate the elbow joint response for ITSE-tuned controllers. Both error-based indices maintain stable performance but exhibit higher oscillatory tendencies than the ITAE and IAE criteria. The ISE and ITSE-tuned controllers exhibit higher oscillatory behavior than the IAE and ITAE-based controllers. They place greater weight on early transient deviations, leading to more aggressive corrective actions that cause sudden overshoot, which is undesirable in any therapeutic exercise. In terms of minimizing the effects of disturbance, ITAE outperforms other functions. Figures 9a and 9b illustrate the response using Z-N for flexion/extension and internal/external rotation, respectively, showing a pronounced overshoot and a prolonged settling time, with noticeable oscillations around the reference position. This confirms that the Z–N method is less suitable for precise rehabilitation control tasks, where smooth motion and safety are critical.

Table 6. Performance Controller Parameters

Controller	Joint	O. S (%)	R.T (s)	S.T (s)	Ms
ACO-PID	Integral Squared Error				
	Extension/ Flexion	16.3%	0.0184	7.83	1.63
	Internal/ External Rotation	1.6%	0.129	16.5	1.23
	Integral Time Squared Error				
	Extension/ Flexion	10%	0.0182	6.2	1.53
	Internal/ External Rotation	1.3%	0.112	7.13	1.21
	Integral Absolute Error				
	Extension/ Flexion	2.08%	0.0569	0.131	1.34
	Internal/ External Rotation	3.8%	0.15	0.558	1.28
	Integral Time Absolute Error				
	Extension/ Flexion	Below 1%	0.0837	0.144	1.28
	Internal/ External Rotation	1.6%	0.234	0.359	1.32
Ziegler Nichols	Extension/ Flexion	78.6%	0.0654	2.47	1.53
	Internal/ External Rotation	40.2%	0.212	2.13	1.33

Table 6 presents the four performance indices for the PID parameters optimized by ACO, compared with the Z-N controller for elbow joint control. The findings highlight the distinct trade-offs of each performance index, providing insight into selecting the most appropriate performance criterion.

The Z-N-tuned controller exhibited a transient response characterized by a pronounced overshoot of 78.6% for elbow extension/flexion and 40.2% for internal/external rotation. Such excessive overshoot is not clinically acceptable in passive rehabilitation, since it may cause injury to the patient. In contrast, all ACO-tuned controllers drastically reduced the overshoot, demonstrating the fundamental advantage of the optimization approach. The Z-N-tuned controller showed a marginally faster rise time of 0.0653s for elbow extension/flexion, with a

settling time of 2.47s and a rise time of 0.234s for internal/external rotation, with a settling time of 2.13s. This represents the apparent speed at the cost of severe overshoot.

Among the four performance indices, the ITAE delivers the most balanced overall performance. For flexion/ extension movement, it achieves an overshoot of approximately 1%, combined with a settling time of 0.144s and a rise time of 1.28s. The maximum sensitivity index $M_s = 1.28$ falls within the accepted range, indicating good disturbance rejection. For internal/ external rotation, it achieves an overshoot of 1.6% with a settling time of 0.359s and a rise time of 0.234s. The $M_s = 1.32$ falls within the acceptable range. This combination of minimal overshoot, a reasonably quick settling time, and robustness makes ITAE a particularly compelling choice for applications where precise trajectory tracking is the predominant factor.

The IAE criterion also performs well, yielding a low overshoot of 2.08% for flexion/extension and the quick settling time of 0.131 s. This suggests that IAE is effective at quickly eliminating errors. However, its M_s value of 1.34 is slightly higher than that of ITAE, pointing to marginally lower robustness, although still within an acceptable range. For internal/external rotation, it exhibits an overshoot of 3.8%, a rise time of 0.15s, and a settling time of 0.558s. The value for M_s is 1.28, showing higher disturbance rejection.

Both quadratic indices produce less favorable transient responses. For the flexion/extension joint, ISE exhibits an overshoot of 16.3% with a rise time of 0.0184s and a settling time of 7.83 s, whereas ITSE exhibits a 10% overshoot with a rise time of 0.182s and a settling time of 6.2s, exhibiting noticeable oscillations. Aggressive corrective action that results from heavily penalizing large errors tends to induce a more nervous, oscillatory behavior, which is the type of response to avoid in a therapeutic context, where smooth, gentle motion is essential. The Ms value of 1.43 for ISE was achieved, whereas the Ms value for ITSE was 1.53, which is in the acceptable range. For internal/external rotation, ISE exhibits an overshoot of 1.6% with a rise time of 0.129s and a settling time of 16.5s, whereas ITSE exhibits a 1.3% overshoot with a rise time of 0.112s and a settling time of 7.13s, both indicating an oscillatory response.

Figure 10a and 10b show the tracking performance of the elbow joint flexion/extension and internal/external rotation when subjected to a sinusoidal reference trajectory. This test is particularly important for rehabilitation applications because sinusoidal motion closely resembles natural rhythmic movements commonly used during passive and assisted therapy sessions. The ACO-tuned controller, based on the ITAE criterion, closely follows the reference signal throughout the cycle, with only a slight deviation near the peak of the oscillation. The small variation settles rapidly, and the trajectory recalibrates with the nominal curve. The transient quickly stabilizes, and the trajectory moves to the intended position almost immediately. The Z-N controller, by contrast, exhibits a predictable phase lag, most pronounced around the ascending and descending zero-crossings. The delay is evidence of decreased responsiveness, even though the Z-N output eventually fully tracks the sinusoidal signal. The added perturbation makes the Z-N controller react significantly faster than the ACO-based approach. Nonetheless, this rapid response comes at the expense of precision, as the Z-N output exhibits steady-state error. In comparison, the ACO-tuned controller achieves superior tracking accuracy and smoothly returns to the reference trajectory, with a small residual error. This is an essential difference in rehabilitation, where rapid but inaccurate responses to situations can result in pain, whereas consistent, correct recovery can guarantee safer, more controlled joint movements.

5. CONCLUSION

This study presents the use of ant colony optimization to tune PID parameters for precise movement control of an elbow exoskeleton for use in the inactive form of forelimb rehabilitation. The proposed model is a synthesis of an Euler-Lagrange formulation that provides a 2-DOF PID structure for setpoint tracking and disturbance rejection, and a continuous-domain ACO algorithm that is employed to find an optimal solution.

The findings show that ACO significantly improves controller performance compared to the traditional Z–N approach. Of the four performance indices compared (ISE, ITSE, IAE, and ITAE), the ITAE criterion yielded the most appropriate performance. The overshoot was reduced from 78.6% (with Z-N) to approximately 1% for elbow flexion/ extension, achieving a settling time of 0.144s, and maintaining sustained disturbance rejection in the presence of simulated patient-induced forces. Similarly, for the internal/external rotation joint, the ITAE-optimized controller limited overshoot to 1.6%, settled in 0.359 s, and delivered an M_s of 1.32—well within the robust range. While the IAE criterion produced the fastest settling time, the ITAE-based controller offered the best overall combination of precision. Additionally, the sinusoidal trajectory was used as a reference, further demonstrating the effectiveness of the proposed method. The ACO-based controller proved useful for monitoring cyclic movements required during rehabilitation exercises, whereas the Z-N controller exhibited lag and steady-state errors.

Although the present study is limited to simulation analysis of the elbow joint on the RAX-1 exoskeleton, future research should focus on hardware implementation, multi-DOF control of the RAX-1 exoskeleton, and clinical tests involving patients with stroke to evaluate its actual performance, safety, and therapeutic effects.

ACKNOWLEDGEMENT

The author of this paper genuinely conveys their heartfelt appreciation for the comprehensive assistance provided by Universiti Kuala Lumpur in successfully concluding this project. This assistance comprised monetary support, the use of other facilities, such as the Intelligent Embedded Research Lab (IERL) research cluster, the experimental laboratory at the UniKL BMI, and the efforts of all contributors.

REFERENCES

[1] Lee SH, et al. (2020). Comparisons between end effector and exoskeleton rehabilitation robots regarding upper extremity function among chronic stroke patients with moderate to severe upper limb impairment. Scientific Reports, 10(1):1-8. https://doi.org/10.1038/s41598-020-58630-2

[2] Mehrholz J, Pollock A, Pohl M, Kugler J, Elsner B. (2020). Systematic review with network meta analysis of randomized controlled trials of robotic assisted arm training for improving activities of daily living and upper limb function after stroke. Journal of NeuroEngineering and Rehabilitation, 17(1):1-14. https://doi.org/10.1186/S12984-020-00715-0

[3] Ranzani R, et al. (2020). Neurocognitive robot assisted rehabilitation of hand function: a randomized control trial on motor recovery in subacute stroke. Journal of NeuroEngineering and Rehabilitation, 17(1):1-13. https://doi.org/10.1186/S12984-020-00746-7

[4] Dalla Gasperina S, Roveda L, Pedrocchi A, Braghin F, Gandolla M. (2021). Review on patient cooperative control strategies for upper limb rehabilitation exoskeletons. Frontiers in Robotics and AI, 8:745018. https://doi.org/10.3389/frobt.2021.745018

[5] Ai Q, Liu Z, Meng W, Liu Q, Xie SQ. (2023). Machine learning in robot assisted upper limb rehabilitation: a focused review. IEEE Transactions on Cognitive and Developmental Systems, 15(4):2053-2063. https://doi.org/10.1109/TCDS.2021.3098350

[6] Escarabajal RJ, Pulloquinga JL, Zamora-Ortiz P, Valera A, Mata V, Valles M. (2023). Imitation learning based system for the execution of self paced robotic assisted passive rehabilitation exercises. IEEE Robotics and Automation Letters, 8(7):4283-4290. https://doi.org/10.1109/LRA.2023.3281884

[7] Brown DF, Xie SQ. (2024). Effectiveness of intelligent control strategies in robot assisted rehabilitation: a systematic review. IEEE Transactions on Neural Systems and Rehabilitation Engineering, 32:1828-1840. https://doi.org/10.1109/TNSRE.2024.3396065

[8] Brahmi B, Driscoll M, El Bojairami IK, Saad M, Brahmi A. (2021). Novel adaptive impedance control for exoskeleton robot for rehabilitation using a nonlinear time delay disturbance observer. ISA Transactions, 108:381-392. https://doi.org/10.1016/j.isatra.2020.08.036

[9] Ranzani R, Chiriatti G, Schwarz A, Devittori G, Gassert R, Lambercy O. (2023). An online method to monitor hand muscle tone during robot assisted rehabilitation. Frontiers in Robotics and AI, 10:1093124. https://doi.org/10.3389/frobt.2023.1093124

[10] Cao J, et al. (2024). Variable admittance control of high compatibility exoskeleton based on human robotic interaction force. Chinese Journal of Mechanical Engineering, 37(1):119. https://doi.org/10.1186/S10033-024-01113-6

[11] Yang R, Zheng J, Song R. (2022). Continuous mode adaptation for cable driven rehabilitation robot using reinforcement learning. Frontiers in Neurorobotics, 16:1068706. https://doi.org/10.3389/fnbot.2022.1068706

[12] Zhou J, Peng H, Zheng M, Wei Z, Fan T, Song R. (2024). Trajectory deformation based multi modal adaptive compliance control for a wearable lower limb rehabilitation robot. IEEE Transactions on Neural Systems and Rehabilitation Engineering, 32:314-324. https://doi.org/10.1109/TNSRE.2023.3348332

[13] Wang Y, Held D, Erickson Z. (2022). Visual haptic reasoning: estimating contact forces by observing deformable object interactions. IEEE Robotics and Automation Letters, 7(4):11426-11433. https://doi.org/10.1109/LRA.2022.3199684

[14] Yang J, Su H, Li Z, Ao D, Song R. (2016). Adaptive control with a fuzzy tuner for cable based rehabilitation robot. International Journal of Control, Automation and Systems, 14(3):865-875. https://doi.org/10.1007/S12555-015-0049-4

[15] Poudel YK, Bhandari P. (2024). Control of the BLDC motor using ant colony optimization algorithm for tuning PID parameters. Archives of Advanced Engineering Science, 2(2):108-113. https://doi.org/10.47852/BONVIEWAAES32021184

[16] Mirrashid N, Alibeiki E, Rakhtala SM. (2022). Development and control of an upper limb rehabilitation robot via ant colony optimization PID and fuzzy PID controllers. International Journal of Engineering, Transactions B Applications, 35(8). https://doi.org/10.5829/IJE.2022.35.08B.04

[17] Biodex. (n.d.). System 3 and 4 upper extremity hemiparetic attachments operation manual. Retrieved from https://www.biodex.com

[18] Joyo MK, et al. (2019). Optimized proportional integral derivative controller for upper limb rehabilitation robot. Electronics, 8(8):826. https://doi.org/10.3390/electronics8080826

[19] Moradi B, Kargar A, Abazari S. (2022). Transient stability constrained optimal power flow solution using ant colony optimization for continuous domains. IET Generation Transmission and Distribution, 16(18):3734-3747. https://doi.org/10.1049/gtd2.12560

[20] Precup R. E., Preitl, S., and Korondi, P. (2007). Fuzzy controllers with maximum sensitivity for servosystems. IEEE Transactions on Industrial Electronics, 54(3):1298–1310. https://doi.org/10.1109/TIE.2007.893053